DOI: 10.1002/chem.200500137

On the Oxidation of Gallium and Indium: Characterization of the Cyclic and Linear GaO_2 and InO_2 Molecules Generated by the Spontaneous and Photoinduced Reaction of Ga and In Atoms with O_2 and Determination of the Reaction Mechanism

Andreas Köhn,[b] Benjamin Gaertner,[a] and Hans-Jörg Himmel*[a]

Abstract: In this work, the spontaneous and photolytically activated reactions of Ga and In atoms (M) with O_2 (in Ar and solid O_2) are studied with the aid of the matrix-isolation technique and the use of IR, Raman, and UV/Vis spectroscopy in combination with detailed quantum-chemical calculations. Vibrational spectra were recorded for several different isotopomers (^{69}Ga, ^{71}Ga, $^{16}O_2$, $^{18}O_2$, $^{16}O^{18}O$). The results show that the spontaneously formed cyclic MO_2 molecules photoisomerize to give the linear OMO molecules. The collected vibrational data were then used to characterize the bond properties of the linear OMO molecules in detail. The results are compared to those obtained for CO_2^+ and neutral OEO compounds, where E is an element of Group 14. Quantum-chemical calculations were carried out at various levels of theory for GaO_2. These calculations indicate that linear OMO is slightly more stable than its cyclic isomer. These calculations were also used to obtain information about the reaction mechanism, and show that the formation of the cyclic isomer from Ga atoms and O_2 occurs without a significant barrier. Abrupt changes of the dipole moment and the O–O bond length during the approach of the O_2 molecule toward the Ga atom mark the point on the potential energy surface at which one electron jumps from the Ga atom onto the O_2 unit. The isomerization of cyclic GaO_2 to the linear global minimum structure is accompanied by a significant barrier, which explains why this reaction requires photoactivation.

Keywords: Group 13 elements · matrix isolation · oxidation · quantum-chemical calculations · reaction mechanisms

Introduction

The knowledge and control of metal-catalyzed oxidation processes is of fundamental as well as industrial interest. In the course of these processes, the bond of O_2, the strength of which amounts to almost 500 kJ mol^{-1}, has to be cleaved. This is achieved by transfer of electron density from the metal atoms into the antibonding π^* orbitals of the O_2. It is now well known that the oxidation of a metal surface generally starts at defects as they exhibit an increased reactivity with respect to the defect-free regions of the surface. These defects contain atoms with a smaller coordination number than the ones in defect-free regions. Our studies aim to answer the question whether, and under what conditions, a single metal atom (being free of neighboring atoms) is capable of weakening considerably, or even breaking, the bond of O_2. In this study we concentrate on the oxidation of Ga and In atoms. Ga and In are widely used for the fabrication of III/V semiconductor devices, and oxidation processes can seriously damage the semiconducting properties of these devices. The blackening of the resonator surfaces of laser diodes represents an impressive example of a highly undesired oxidation reaction that can ultimately lead to the phenomenon of "catastrophic optical mirror damage".[1]

The reactions of Ga and In atoms with O_2 have already been studied with the aid of the matrix-isolation technique. As early as 1979 Carlson et al. studied the spontaneous reaction of matrix-isolated Ga and In (M) atoms with O_2 by IR

[a] Dr. B. Gaertner, Priv. Doz. Dr. Dr. H.-J. Himmel
Institut für Anorganische Chemie, Universität Karlsruhe (TH)
Engesserstrasse Geb. 30.45, 76128 Karlsruhe (Germany)
Fax: (+49) 721-608-4854
E-mail: himmel@chemie.uni-karlsruhe.de

[b] Dr. A. Köhn
Institut für Nanotechnologie, Forschungszentrum Karlsruhe
Postfach 3640, 76023 Karlsruhe (Germany)
Present address: Department of Chemistry, Århus University
Langelandsgade 140, 8000 Århus (Denmark)

Supporting information for this article is available on the WWW under http://www.chemeurj.org/ or from the author.

spectroscopy.[2] They identified the cyclic, C_{2v}-symmetric MO_2 superoxo complexes as products of these reactions. A few years later (1982), Serebrennikov et al. confirmed these results.[3] However, these experiments failed to give clear evidence for any Ga isotopic splitting, and therefore the exact composition of the superoxo complex remained uncertain. In addition, the spectra only show miniscule and uncertain signs of the symmetric ν(M–O) stretching fundamental. In both studies the metal atoms were generated from resistively heated evaporators. In 1992, Andrews et al. reported the reactions of laser-ablated Ga and In atoms with O_2.[4] In addition to the bands observed previously that were assigned to superoxo complexes, an extra band which grew in intensity upon photolysis was observed for both the Ga and the In reactions. These bands were assigned to the linear OGaO and OInO molecules on the basis of the gallium and oxygen isotopic patterns and hybrid-DFT calculations.[5]

Several quantum-chemical calculations have been reported on the structure and vibrational spectra of the cyclic superoxo complex GaO_2.[6,7] These calculations suggested a $^2A_2$ electronic ground state with C_{2v} symmetry. It turned out, however, that the correct inclusion of electron correlation is important. Thus, while the geometries calculated with different methods differ only slightly, the IR properties and the dissociation energies vary to a large extent depending on the method used.

Quantum-chemical calculations on the linear OGaO species are sparse. So far, to the best of our knowledge, only hybrid-DFT (B3LYP) calculations have been reported in the literature.[5] In these calculations, the wavenumber calculated for the antisymmetric stretching fundamental is about 150 cm^{-1} lower than the experimentally observed wavenumber. Thus, the linear molecule is not fully characterized in experiments or in calculations. Calculations on the reaction mechanism leading to cyclic or linear GaO_2 have also not been carried out so far.

Our study aims at a more complete characterization of the cyclic and linear GaO_2 and InO_2 molecules. We report the first Raman spectra of InO_2, and the symmetric ν(M–O) fundamentals of both cyclic species are detected with certainty for the first time. In addition, the high-resolution spectra measured for the cyclic GaO_2 molecule give the first evidence for an isotopic splitting due to the ^{69}Ga and ^{71}Ga isotopes, which clearly shows the presence of one Ga atom in the compound. The linear OGaO and OInO molecules can be formed from the cyclic GaO_2 and InO_2 isomers by photolysis. The bending modes of both molecules, which provide direct information about the bond properties, are also detected for the first time. The electronic properties of these species will be discussed in detail on the basis of the experimental results and the results of quantum-chemical calculations. This discussion also includes a comparison with CO_2^+ and other neutral EO_2 species, where E is a Group 13 or 14 element. Finally, quantum-chemical calculations are employed to retrieve information about the reaction mechanism.

Experimental Section

Ga was evaporated from a resistively heated carbon cell placed inside an alumina tube. The Ga vapor was co-deposited together with O_2 or Ar doped with O_2 onto a copper block which was kept at a temperature of 10 K by means of a closed-cycle refrigerator (Leybold LB115). $^{16}O_2$ was used as delivered by Messer. $^{18}O_2$ was purchased from Linde (isotopic purity 99.0%). $^{16}O^{18}O$ was prepared by discharge of a 1:1 mixture of $^{16}O_2$ and $^{18}O_2$, followed by condensation of O_3 in a 77 K cold trap and decomposition to reform O_2. Details of the matrix-isolation technique can be found elsewhere.[8]

IR spectra were measured on a Bruker 113v spectrometer. An MCT detector was used for measurements in the spectral range 4000–650 cm^{-1}. A bolometer was used for measurements in the region 700–30 cm^{-1}. Generally, the spectra were recorded with a resolution of 0.1 cm^{-1}.

Raman spectra were recorded with a Jobin Yvon XY spectrometer equipped with a CCD camera (Wright Instruments, England). The spectrometer contained two grids as pre-monochromator and another one as spectrograph; the measurements were preformed in the subtractive mode. The 513.5, 488.0, and 457.9 nm lines of an Ar^+ ion laser (Coherent, Innova 90) were used for excitation. All spectra were recorded with a resolution of 0.5 cm^{-1}.

UV-photolysis was achieved with the aid of a medium-pressure Hg lamp (Firma Graetzel, Karlsruhe, Germany).

UV/Vis spectra were recorded with a Xe arc lamp (Oriel), an Oriel multispec spectrograph, and a photodiode array detector, with a resolution of 0.5 nm.

Details of the quantum-chemical calculations: Calculations were performed with the aid of the program packages TURBOMOLE,[9] DALTON,[10] and MOLPRO.[11] With TURBOMOLE, hybrid-DFT (B3LYP)[12] calculations in combination with a TZVPP basis set[13a] were carried out. The program package DALTON was used for complete active space self-consistent field (CASSCF) calculations. Finally, the MOLPRO program package was employed for coupled-cluster and multi-reference configuration-interaction (MR-CI) calculations. For all the latter calculations a TZVPP basis set was used for the oxygen atom, with an extended extTZVPP basis set, as described in reference [14], for the gallium atom. The effect of diffuse basis functions on oxygen was tested at the DFT level and found to be unimportant, provided basis sets of triple-zeta quality are used.

DFT calculations were carried out for both GaO_2 and InO_2. In the latter case the relativistic effective core potential (ECP) of the Stuttgart group was used for In, thereby incorporating scalar relativistic effects into the calculation. Spin-orbit effects were not included.[13b,c]

The CCSD(T) calculations[15] included, in all cases, the correlation of the d-electrons of gallium, but the remaining core of gallium and the 1s core of oxygen were excluded from the correlation treatment (frozen-core approximation). The calculations were based on restricted open-shell Hartree–Fock (ROHF) orbitals, but in the coupled-cluster calculations no spin-symmetry constraints were imposed on the cluster amplitudes (unrestricted coupled-cluster). The spin-contaminations were monitored, but turned out to be small. Geometries were optimized numerically at this level and the second derivatives were also obtained numerically.

The active space for CASSCF calculations was chosen to accommodate all valence orbitals; 15 electrons in 12 orbitals were included in total. While this choice is optimal for the linear GaO_2 compound, we observed that for the cyclic isomers some of the weakly occupied orbitals assume diffuse oxygen 3p character instead of the intended Ga 3p character as dynamical correlation effects dominate in these species. As a consequence, the cyclic isomer is over-stabilized in the CASSCF calculations. A balanced extension of the active space turned out to be difficult, as localization artifacts in the linear isomer, which lead to unphysical second derivatives for the anti-symmetric stretching mode, occur for any tractable size even of restricted active space SCF (RASSCF) calculations. We therefore did not construct an active space that is balanced over the whole potential energy surface discussed. We shall, however, bring the following issues to the attention of the reader:

a) Any discussion of the thermal reaction path between the linear and the cyclic isomer based on CASSCF calculations can only be of qualitative nature. The arguments for a sizeable barrier (vide infra) seem, however, clear-cut enough for the current purposes.

b) The active space for the cyclic isomer is not consistent with that of the separated gallium atom and dioxygen molecule as the calculated reaction energy based on CASSCF turns out to be much too high. We will not include these numbers in the discussion as more-reliable numbers are available from CCSD(T) calculations.

c) The reaction path of the $O_2(^3\Sigma_g^-)+Ga(^2P)$ reaction was calculated using the RASSCF approach[16] instead: The active space was extended to formally include all 3p orbitals of the oxygen atoms, thus ensuring a smooth hypersurface for all separations of the Ga and O_2 fragments considered. This active space includes 18 orbitals and 15 electrons. To keep the calculations computationally feasible, the active space was subdivided into three subspaces: RAS1, which comprises six orbitals of which at most two electrons may be excited, RAS2 (five orbitals, including all Ga 3p, and the O_2 π_g* orbitals), without restriction on the number of electrons, and RAS3, which may accommodate two electrons at most.

The MR-CI calculations were based on the CASSCF orbitals and the valence active space described above. The CI was carried out among all singly and doubly excited configurations out of the reference configurations by keeping the doubly external configurations internally contracted as implemented in the MOLPRO CI-program.[11e] For some of the MR-CI calculations, the reference configurations were pre-selected according to their weight in the CAS wavefunction. A threshold of 0.01 was used and an estimate of the error arising will be given later in the text. Finally, to account for the size-extensivity error in CI calculations, both the Davidson correction[17] and the modified CI procedures ACPF[18] and AQCC[19] were used. Calculations with and without correlation contributions from the d electrons were carried out; the remaining core electrons were not included in the correlation treatment.

Finally, we note that all calculations refer to the gas phase; that is, environment effects, such as those from the inert gas matrix, were not included, which has to be kept in mind when comparing the results with experimental data. Likewise, only harmonic vibrational normal modes and frequencies were calculated, whereas reported experimental numbers are the anharmonic fundamental frequencies of the molecular vibrations.

Results

In the following sections the experimental results will be reported in turn first for Ga and then for In. The results of the quantum-chemical calculations will be presented in the discussion. Their aim is to lend support to the identification of the reaction products, to further characterize these species, and to analyze the mechanisms leading to their formation.

$Ga+O_2$

IR: Figure 1 shows the IR spectra recorded for a matrix of solid Ar at 10 K containing Ga atoms and 1% of $^{16}O_2$. The spectrum taken immediately after deposition shows three sharp absorptions, located at 1089.3, 380.5/378.9, and 283.2 cm^{-1}, which can be assigned to a first, spontaneously formed product **1a** of the reaction between Ga atoms and $^{16}O_2$. The splitting of the band near 380 cm^{-1} is caused by the presence of two isotopomers due to the presence of ^{69}Ga and ^{71}Ga (natural abundance of 0.601 and 0.399, respectively). The relative intensities of the two bands indicate the presence of only one Ga atom in **1a**. Photolysis of the matrix with UV radiation ($\lambda_{max}=254$ nm) leads to the decay

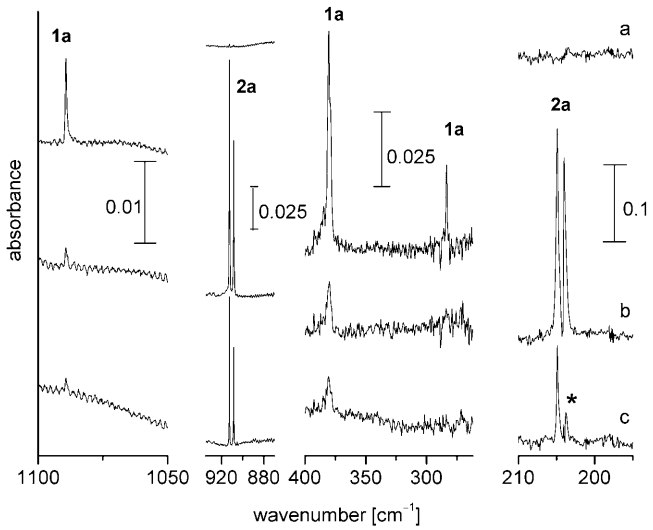

Figure 1. IR spectra taken for an Ar matrix containing Ga atoms and 1% $^{16}O_2$: a) upon deposition, b) following 10 min of photolysis at $\lambda_{max}=$ 254 nm, and c) upon annealing of the matrix to 30 K. Unfortunately, an overtone of 50 Hz overlaps with the band marked with an asterisk, which affects its intensity.

of the absorptions due to species **1a** and the simultaneous appearance of a sharp doublet feature at 912.6/908.6 cm^{-1} in the MIR region and a strong doublet feature at 204.9/204.0 cm^{-1} in the FIR region (trace b in Figure 1). The doublet patterns of these bands again most likely arise from $^{69}Ga/^{71}Ga$ isotopic splitting and display relative intensities that mirror the natural relative abundance of ^{69}Ga and ^{71}Ga satisfactorily. The two absorptions belong to a second product (**2a**), and the experiments indicate that **1a** is the precursor to **2a**. The doublet pattern of the absorption at 912.6/908.6 cm^{-1} is due to isotopic splitting (^{69}Ga and ^{71}Ga). This isotopic splitting has already been reported.[4] In agreement with this earlier work, we conclude that **2a** (like **1a**) most likely contains a single Ga atom. Annealing of the matrix caused the bands of **2a** to decrease in intensity.

The experiment was repeated, but this time in solid $^{16}O_2$. Again, bands belonging to a single, spontaneously formed product of the reaction between Ga atoms and O_2 are visible in the IR spectrum taken directly upon deposition. These bands are located at 1087.4, 380.2, and 288.8 cm^{-1} and are close to the ones observed in the experiments conducted in an Ar matrix. The obvious inference is that the same product is formed. Thus, **1a** does not react spontaneously with additional O_2 molecules under the conditions of the matrix-isolation experiments. Upon photolysis with light at $\lambda_{max}=254$ nm, the bands due to **1a** again decrease. However, this time no bands belonging to product **2a** were detected. Instead, a different species—the product of the reaction of Ga with not one, but two O_2 molecules—is formed. This product, with the overall formula GaO_4, is the topic of a separate paper.[20] These results imply that **2a**, once formed, reacts spontaneously with additional O_2 molecules. Bands due to O_3, which is formed by photodecomposition of O_2

and its subsequent reaction with the O atoms, also appear in the spectra.

Additional experiments were conducted with different O_2 isotopomers, again in Ar matrices. Figure 2 shows the spectra obtained for $^{16}O_2$ (a), $^{18}O_2$ (b), a 1:1 mixture of $^{16}O_2$ and $^{18}O_2$ (c), and a 1:2:1 mixture of $^{16}O_2$, $^{16}O^{18}O$, and $^{18}O_2$ (d) in an Ar matrix. The spectra in the regions 1100–1020 and 400–270 cm^{-1} were taken immediately upon deposition and contain the absorptions due to species **1a**. The spectra in the regions 915–870 and 210–190 cm^{-1} were taken after photolysis of the matrix at $\lambda_{max}=254$ nm and contain the absorptions typical for **2a**. In the experiments with $^{18}O_2$, the bands due to **1a** and **2a** are red-shifted to 1027.9, 365.9/364.5, and 268.1 cm^{-1}, and 877.6/873.4 and 197.3/196.3 cm^{-1}, respectively. The spectrum measured in the experiment with an almost equimolar mixture of $^{16}O_2$ and $^{18}O_2$ is essentially a superposition of the spectra obtained for $^{16}O_2$ and $^{18}O_2$ alone. Finally, in the experiment with a 1:2:1 mixture of $^{16}O_2$, $^{16}O^{18}O$, and $^{18}O_2$, extra bands are observed at 1059.0, 373.6/372.2, and 275.3 cm^{-1} (**1a**) and 897.4/893.4 and 201.1/200.1 cm^{-1} (**2a**). From the number of bands it can be directly concluded that **1a** and **2a** contain two chemically equivalent O atoms. In this we agree with earlier reports.[3,4] Thus, both **1a** and **2a** exhibit the overall formula GaO_2. It is worth mentioning that the band due to the $^{16}O^{18}O$ isotopomer of **2a** at 897.4/893.4 cm^{-1} is slightly blue-shifted with respect to the center of the bands measured for the $^{16}O_2$ and $^{18}O_2$ isotopomers (which is at 895.1/891.0 cm^{-1}). This indicates that the symmetric stretching mode lies at lower frequency, as will be discussed below. Table 1 contains a list of wavenumbers for all bands assigned to **1a** and **2a**, together with their behavior upon photolysis and annealing.

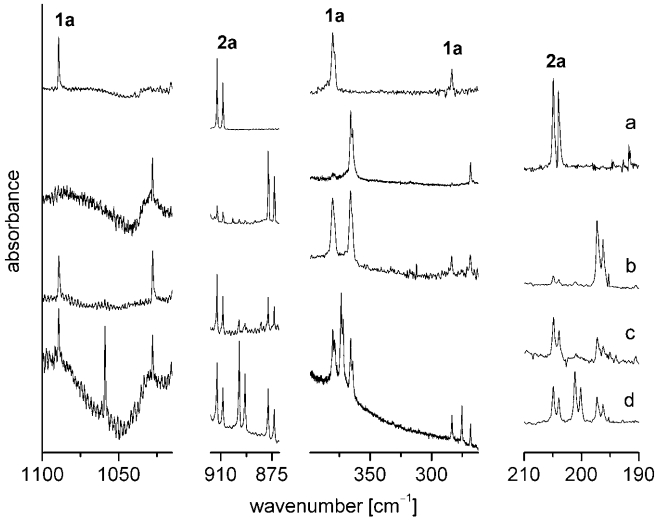

Figure 2. IR spectra taken for the reaction between Ga atoms and $^{16}O_2$ (a), $^{18}O_2$ (b), a 1:1 mixture of $^{16}O_2$ and $^{18}O_2$ (c), and a 1:2:1 mixture of $^{16}O_2$, $^{16}O^{18}O$, and $^{18}O_2$ (d) in an Ar matrix. The spectra in the regions 1100–1020 and 400–270 cm^{-1} were taken after deposition. The spectra in the regions 915–870 and 210–190 cm^{-1} were taken after photolysis.

Table 1. Observed wavenumbers [cm^{-1}] for the reaction between Ga atoms and O_2 in Ar and in solid O_2 matrices.[a]

Ga/O_2 in Ar			Ga/O_2		Dep.	Photolysis ($\lambda_{max}=254$ nm)	Anneal. (30 K)	Absorber
$^{16}O_2$	$^{16}O^{18}O$	$^{18}O_2$	$^{16}O_2$	$^{18}O_2$				
1089.3	1059.0	1027.9	1087.4	1026.0	↑	↓	↓	**1a**
912.6/908.5	897.4/893.4	877.6/873.4	–	–	–	↑	↓	**2a**
380.5/378.9	373.6/372.2	365.9/364.5	380.2	364.9	↑	↓	↓	**1a**
283.2	275.3	268.1	288.8	273.1	↑	↓	↓	**1a**
204.9/204.0	201.1/200.1	197.3/196.3	–	–	–	↑	↓	**2a**

[a] ↑: increase in intensity; ↓: decrease in intensity.

Raman: In further experiments, Raman spectra were recorded. For low concentrations of O_2 in the matrix, the spectra show no product signal; only for increased O_2 concentrations (3 % O_2 in Ar) did a sharp signal appear at 716.2 cm^{-1}. However, experiments in which the O_2 concentration in the matrix was systematically varied showed that this signal does not belong to **1a** or **2a**, but to a third species, which will be discussed in a separate paper.[20]

UV/Vis: UV/Vis spectra were recorded in the hope of observing an electronic absorption of **1a** or **2a**. A strong and sharp absorption at $\lambda=345$ nm belongs to Ga atoms ($^2S\leftarrow{}^2P$ electronic transition) and a weaker feature around $\lambda=412$ nm can be assigned to Ga_2.[21,22] The band at 345 nm undergoes a sharp decrease in intensity upon photolysis. However, no other band assignable to a product of the reaction of Ga or Ga_2 with O_2 is visible.

In + O_2

IR: The IR spectra of an Ar matrix containing In and 1 % $^{16}O_2$ are displayed in Figure 3. Figure 3a shows the spectrum taken immediately after deposition. As in the case of the Ga reaction, three bands are visible in this spectrum, thus showing that In reacts spontaneously with O_2. These bands are located at 1084.2, 331.7, and 276.5 cm^{-1} and can all be assigned to a single product (**1b**). Figure 3b shows the spectrum obtained after a period of 10 min of photolysis at $\lambda_{max}=254$ nm. The bands due to **1b** are observed to decrease significantly in intensity. At the same time, two new bands at 754.6 and 159.7 cm^{-1} grow-in. These two bands can be assigned to a second product (**2b**) of the reaction between In and O_2. The positions of the bands of the two species and the conditions of their growth and decay indicate that **1b** and **2b** are the In analogues of **1a** and **2a**.

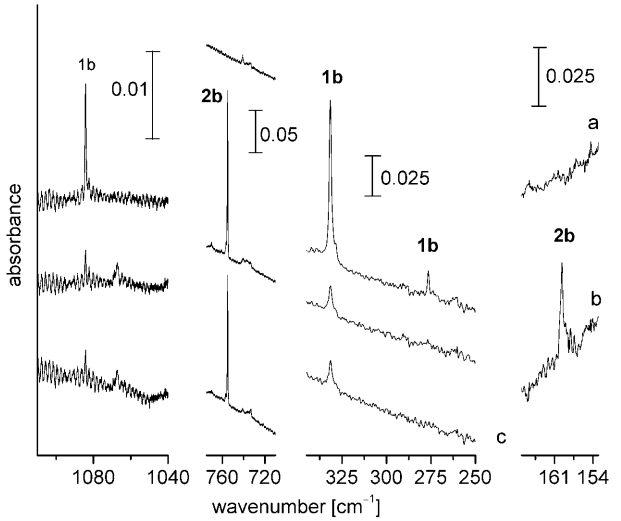

Figure 3. IR spectra taken for an Ar matrix containing In atoms and 1 % $^{16}O_2$: a) upon deposition, b) following 10 min of photolysis at λ_{max} = 254 nm, and c) upon annealing of the matrix to 30 K.

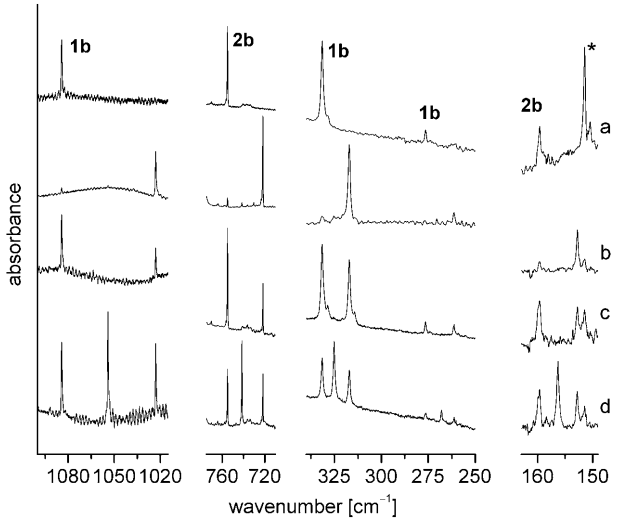

Figure 4. IR spectra taken for the reaction between In atoms and $^{16}O_2$ (a), $^{18}O_2$ (b), a 1:1 mixture of $^{16}O_2$ and $^{18}O_2$ (c), and a 1:2:1 mixture of $^{16}O_2$, $^{16}O^{18}O$, and $^{18}O_2$ (d) in an Ar matrix. The spectra in the regions 1100–1020 and 400–270 cm^{-1} were taken after deposition. The spectra in the regions 915–870 and 210–190 cm^{-1} were taken after photolysis.

An additional experiment was carried out for In isolated in a solid $^{16}O_2$ matrix. The spectrum taken for this experiment again shows three bands, located at 1082.8, 331.7, and 283.5 cm^{-1}, upon deposition. Their positions are close to those observed for **1b** in an Ar matrix and thus the obvious inference is that they also belong to a similar product. Photolysis of the matrix causes the three bands to decrease until they almost vanish. No bands in regions typical of **2b** can be observed. Instead, other features belonging to a third species are seen to grow-in. This species is the product of the reaction of In with two O_2 molecules and will be discussed in a separate paper together with its Ga analogue.[20] As in the case of the Ga reaction, it can be concluded that **1b** does not react spontaneously with additional O_2 molecules, while **2b**, once formed, does react further.

The results of the experiments with different O_2 isotopomers in an Ar matrix are contained in Figure 4. Replacement of $^{16}O_2$ by $^{18}O_2$ leads to a significant red shift of all the absorptions due to **1b** and **2b**. Thus, product **1b** shows bands at 1022.9, 317.2, and 261.3 cm^{-1}, and product **2b** in its ^{18}O form shows bands at 721.7 and 152.8 cm^{-1}. In the experiment with a 1:1 mixture of $^{16}O_2$ and $^{18}O_2$, no additional bands are visible, in agreement with the assumption that **1b** and **2b** contain two chemically equivalent O atoms. In these findings we agree with reference [4]. In the case of experiments with a 1:2:1 mixture of $^{16}O_2$, $^{16}O^{18}O$, and $^{18}O_2$, additional absorptions occur at 1054.0, 325.2, and 267.8 cm^{-1} for **1b** and at 741.4 and 156.3 cm^{-1} for **2b**. Again, the band measured for the $^{16}O^{18}O$ isotopomer of **2b** at 741.4 cm^{-1} is slightly blue-shifted from the midpoint between the bands of the $^{16}O_2$ and $^{18}O_2$ isotopomers (located at 738.2 cm^{-1}). Table 2 contains the wavenumbers of all observed bands due to **1b** and **2b** together with their response to photolysis and annealing.

Table 2. Observed wavenumbers [cm^{-1}] for the reaction between In atoms and O_2 in Ar and in solid O_2 matrices.

In/O_2 in Ar				In/O_2	Dep.	Photolysis (λ_{max}=254 nm)	Anneal. (30 K)	Absorber[a]
$^{16}O_2$	$^{16}O^{18}O$	$^{18}O_2$	$^{16}O_2/^{18}O_2$	$^{16}O_2$				
1084.2	1054.0	1022.9	1.059	1082.8	↑	↓	–	**1b**
754.6	741.4	721.7	1.046	–	–	↑	–	**2b**
331.7	325.2	317.2	1.046	331.7	↑	↓	–	**1b**
276.5	267.8	261.3	1.058	283.5	↑	↓	–	**1b**
159.7	156.3	152.8	1.045	–	–	↑	–	**2b**

[a] ↑: increase in intensity; ↓: decrease in intensity.

Raman: Figure 5 displays the Raman spectrum measured for an Ar matrix containing In and 0.1 % $^{16}O_2$. Three signals are visible whose positions are similar to those found in the IR spectra and can therefore be assigned to **1b**. As anticipated, the relative intensities of the three signals differ from those in the IR spectra. Thus, the signal at 1084.2 cm^{-1} gains in intensity relative to the one at 331.7 cm^{-1}. Upon photolysis, the three signals disappear. No signal due to a second product with the overall formula InO_2 grows-in.

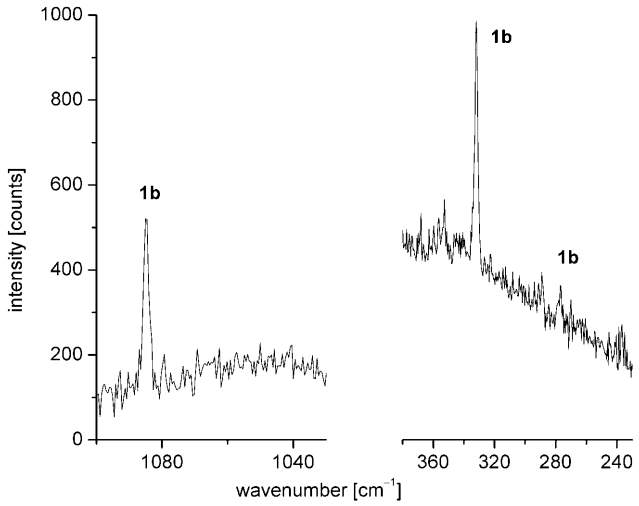

Figure 5. Raman spectrum taken upon deposition of In atoms together with $^{16}O_2$ in an Ar matrix.

Discussion

The accumulated experimental data clearly show that **1a/1b** and **2a/2b** exhibit the overall formula GaO_2 and InO_2, respectively. In previous work, bands due to **1a/1b** have already been assigned to the cyclic MO_2 molecules[2,3] and one band due to **2a/2b** to linear OMO molecules.[4] Nevertheless we start our discussion here with a theoretical survey of possible structures of a molecule with the overall formula MO_2. On the basis of this survey and the experimental results we can then characterize products **1a/1b** and **2a/2b**. The discussion of the bond properties will include the inspection of the force constants obtained from normal mode analysis and high-level multireference studies on the relative energies. Finally, we present results of quantum-chemical calculations, which shed light on the reaction mechanisms leading to these species.

Possible structures of MO_2 (M=Ga or In)

Four minima were found on the potential energy surface due to a cyclic side-on (**A**) or end-on (**B**) coordinated superoxo complex, a side-on coordinated peroxo complex (**C**), and a linear OMO arrangement (**D**). In the following, our discussion will mostly concentrate on the Ga species, since our calculations for In are more qualitative in nature, as spin-orbit splitting might also be of significance for these open-shell molecules. Table 3 compares the calculated distances and bond angles, the energies relative to Ga atoms and O_2, and the calculated harmonic wavenumbers for the four isomers (M = Ga). It turns out that isomers **A** and **D** are clearly the most likely candidates for the most stable isomer as they differ in energy by only 10–20 kJ mol^{-1}. Whereas DFT/B3LYP finds **A** to be more stable, CCSD(T) predicts the linear isomer **D** to be the global minimum. We will elaborate on this issue in Section 3 of this discussion.

Isomer **A** exhibits a $^2A_2$ electronic ground state. The unpaired electron resides in a molecular orbital, which can roughly be described as a π^* orbital at the O_2 unit oriented perpendicularly to the molecular plane. Relative to the neutral fragments, one electron has been transferred from Ga to the O_2 unit. Therefore, we may describe the molecule as a superoxo compound. The O_2 distance is about 15 pm longer than the distance in uncoordinated O_2.

The end-on coordinated superoxo complex GaOO (**B**) has a $^2A'$ electronic ground state and its energy is, according to CCSD(T) calculations, 72 kJ mol^{-1} higher than that of the cyclic superoxo compound **A**. The molecule is not linear, and has a Ga-O-O angle of 128° (according to CCSD(T) cal-

Table 3. Relative energies [kJ mol^{-1}], bond lengths [pm], bond angles [°], and wavenumbers (cm^{-1}, with calculated IR intensities in km mol^{-1} and experimental relative intensities given in parentheses) for different isomers of GaO_2.

Isomer		Exp.	B3LYP	CASSCF	CCSD(T)
	energy rel. to Ga + O_2	–	−207	−232	−215
	d(Ga–O)	–	208	206	204
	d(O–O)	–	134	138	136
A ($^2A_2$)	∢(OGaO)	–	38	39	39
	$\nu_1(a_1)$	1089.3(15)	1172.3(7)	1090.5(1)	1112.2
	$\nu_2(a_1)$	380.1(100)	385.8(86)	415.1(104)	369.8
	$\nu_3(b_1)$	283.2(14)	287.0(9)	297.0(8)	419.1
	energy rel. to Ga + O_2		−151	−186	−143
	d(Ga–O)		189	189	187
	d(O–O)		132	137	134
B ($^2A'$)	∢(GaOO)		141	124	128
	$\nu_1(a')$		1162.3(7)	1070.9(101)	–
	$\nu_2(a')$		436.5(97)	491.4(136)	–
	$\nu_3(a')$		102.9(0)	139.5(1)	–
	energy rel. to Ga + O_2		−41	−101	−89
	d(Ga-O)		182	182	180
C ($^2A_1$)	d(O–O)		163	168	167
	∢(OGaO)		53	55	55
	$\nu_1(a_1)$		788.7(3)	754.6(10)	–
	$\nu_2(a_1)$		578.7(17)	498.3(24)	–
	$\nu_3(b_1)$		553.5(31)	614.1(14)	–
	energy rel. to Ga + O_2		−200	−185	−225
	d(Ga-O)		170	172	170
D ($^2\prod_g$)	∢(OGaO)		180	180	180
	$\nu_1(\Sigma_g)$	821[a]	749.7(0)	720.1(0)	738.2
	$\nu_2(\prod_u)$	204.9	188.4(78), $\varepsilon = 0.07$[b]	182.0(55), $\varepsilon = 0.33$[b]	175.3, $\varepsilon = 0.08$[b]
	$\nu_3(\Sigma_u)$	912.6	647.8(721)	989.6(252)	527.1

[a] Estimated on the basis of the observed isotopic data. [b] Center of Renner–Teller band system, calculated as $\nu_2 = \sqrt{1/2(\nu_{2x}^2 + \nu_{2y}^2)}$; ε: Renner parameter, intensities from sum over both directions.

culations). Although the coordinating end of O_2 is much closer to the metal nucleus than in the side-on coordinated complex **A**, both the lower reaction energy and the shorter O–O bond length of 134 pm suggest a weaker Ga–O_2 interaction in **B**. We note that the calculations indicate that the $^2A''$ hypersurface already lies at lower energy at the equilibrium geometry of **B**. This hypersurface leads, without a further barrier, directly to isomer **A**, such that we must conclude that **B** is unstable with respect to internal conversion.

In the case of isomer **C**, a second electron has been transferred from Ga to O_2 to form a cyclic GaO_2 peroxo species. The compound has a $^2A_1$ electronic ground state, with the unpaired electron now located in a Ga 4s orbital. In agreement with this description, the O–O distance is significantly longer (167 pm) and the Ga–O distance shorter (180 pm) than in **A** or **B**. The energy of **C** works out to be 126 kJ mol^{-1} higher than that of **A**. Again, there are indications that this isomer is very unstable. At all levels of theory, the potential energy curve for the $^2A_2$ state, corresponding to the superoxo complex, and the $^2A_1$ state intersect close to the minimum of the $^2A_1$ curve. This implies that the barrier for reformation of the superoxo complex from the peroxo complex is minuscule (lower than the zero-point vibrational energy) and efficient internal conversion to the superoxo compound can be expected.

Finally, isomer **D** features two terminal Ga–O bonds. The linear molecule has a $^2\prod_g$ ground state,[5] and its Ga–O distance of 170 pm is shorter than in any other isomer. It might come as a surprise that, as noted above, the energy as calculated with CCSD(T) is 10 kJ mol^{-1} lower than that of **A**. It should be mentioned that OGaO is valence isoelectronic with the well known $[OCO]^+$ ion (see below).

For M = In (see Table 4), we find roughly the same trends. The calculations indicate that the cyclic superoxo species **A** is now the global minimum. The end-on superoxo compound **B** is now nearly linear and again unstable with respect to internal conversion to isomer **A**. The same is the case for the peroxo compound, which again lies at highest energy.

Table 4. Relative energies [kJ mol^{-1}], bond lengths [pm], bond angles [°], and wavenumbers (in cm^{-1}, with calculated intensities in km mol^{-1} and experimental relative intensities given in parentheses) for different isomers of InO_2.

Isomer		Exp.	B3LYP
	energy rel. to In + O_2		212
	d(In–O)		217
	d(O–O)		134
A ($^2A_2$)	∢(OInO)		36
	$\nu_1(a_1)$	1084.2(13)	1170.3(5)
	$\nu_2(a_1)$	331.7(100)	352.3(71)
	$\nu_3(b_1)$	276.5(14)	310.6(9)
	energy rel. to In + O_2		156
	d(In–O)		198
	d(O–O)		131
B ($^2A'$)	∢(InOO)		166
	$\nu_1(\Sigma_g)$		1221.5(3)
	$\nu_2(\prod_u)$		379.0(74)
	$\nu_3(\Sigma_u)$		250.0(4)
	energy rel. to In + O_2		49
	d(In–O)		192
	d(O–O)		161
C ($^2A_1$)	∢(OInO)		49
	$\nu_1(\Sigma_g)$		756.9(1)
	$\nu_2(\prod_u)$		581.3(12)
	$\nu_3(\Sigma_u)$		541.4(31)
	energy rel. to In + O_2		184
	d(In–O)		182
	∢(OInO)		180
D ($^2\prod_g$)	$\nu_1(\Sigma_g)$	720[a]	705.8(0)
	$\nu_2(\prod_u)$	159.7(20)	177.7(95), $\varepsilon = 0.05$[b]
	$\nu_3(\Sigma_u)$	754.6(100)	599.0(657.7)

[a] Estimated on the basis of the observed isotopic data (see text for further explanation). [b] Center of Renner–Teller band system, calculated as $\nu_2 = \sqrt{1/2(\nu_{2x}^2 + \nu_{2y}^2)}$; ε: Renner parameter, intensities estimated from sum over both directions.

Identification of the products formed in the matrix reactions

*Cyclic MO_2 (**1a** and **1b**)*: Our experiments show, in agreement with earlier reports, that matrix-isolated Ga and In atoms react spontaneously with O_2. In the case of the In reaction, all three fundamentals of the product were observed for the first time both by IR and Raman spectroscopy. In the case of the Ga reaction, the first detection of an isotopic pattern for one of the bands of **1a** proves that **1a** contains a single Ga atom. Together with the results of the experiments with different O_2 isotopomers, it can be concluded that both **1a** and **1b** exhibit the overall formula MO_2 (M = Ga or In). Since all three bands of **1a** and **1b** are visible in the IR experiment, the two molecules cannot be linear. This is also in agreement with the detection of all three vibrations of **1b** in the Raman spectrum. In addition, the IR spectra show that the two O atoms in **1a** and **1b** are chemically equivalent, and on these grounds **1a** and **1b** should exhibit C_{2v} symmetry. On the basis of our calculations **1a** and **1b** can therefore be assigned to the cyclic superoxo complexes GaO_2 and InO_2 (structural type **A**) with A_2 electronic ground states. This is also in agreement with previous work for which, however, the vibrational data set was less complete. The bands at 1089.3 cm^{-1} for GaO_2 and 1084.2 cm^{-1} for InO_2 can be assigned to the ν(O–O) fundamental $\nu_1(a_1)$. Their position is close to those observed for other superoxo complexes (e.g. of the alkali metals).[23] As expected, this mode gives a strong signal in the Raman spectra and a weak band in the IR spectra, and it exhibits the largest $\nu(^{16}O)/\nu(^{18}O)$ ratio (1.059) of all bands. This ratio is only slightly smaller than that of unperturbed O_2 (1.061). The band at 380.1/378.9 cm^{-1} in the experiments with Ga should belong to the symmetric Ga–O stretch $\nu_2(a_1)$. In contrast to the ν(O–O) mode, this mode is expected to exhibit an isotopic splitting due to $^{69}GaO_2$ and $^{71}GaO_2$, and our experiments indeed give evidence for this splitting, which amounts to 1.2 cm^{-1}. The corresponding band for InO_2 occurs at 331.7 cm^{-1}. The antisymmetric Ga–O stretch, $\nu_3(b_1)$, is detected at 283.2 cm^{-1}.

This band is weak and therefore our experiments were unfortunately not able to detect with certainty any isotopic splitting. The corresponding mode for InO_2 appears at 276.5 cm^{-1}. This assignment is in agreement with the Raman intensities. Tables 3 and 4 compare the observed wavenumbers for cyclic GaO_2 and InO_2 of structure type **A** with those calculated using the B3LYP (for both InO_2 and GaO_2) and CASSCF and CCSD(T) (GaO_2 only) methods. The agreement between experiment and calculation is, in general, pleasing. Among the different methods applied to GaO_2, the B3LYP and CASSCF results are closest to the experimental values (bear in mind that anharmonicity effects were not included in the calculations). The CCSD(T) result for the antisymmetric stretching mode comes out too high (as in the calculations of Archibong et al.[7]), as this mode is affected by an instability of the underlying ROHF wavefunction. The B3LYP results for InO_2 show similar deviations from the experimental values as for GaO_2. On the other hand, the wavenumbers calculated for the other structures (**B**, **C**, and **D**) are clearly in disagreement with the observed ones. Thus, there can be no doubt that **1a** and **1b** are the superoxo complexes **A** with a $^2A_2$ electronic state.

*Linear OMO (**2a** and **2b**)*: The experiments indicate that the bands of **2a** at 912.6/908.5 and 204.9/204.0 cm^{-1} and of **2b** at 754.6 and 159.7 cm^{-1} should also exhibit the overall formula MO_2. The isotopic patterns measured in the experiments using mixtures of $^{16}O_2$ and $^{18}O_2$ and of $^{16}O_2$, $^{16}O^{18}O$, and $^{18}O_2$ clearly show that the two O atoms are chemically equivalent, therefore **2a** and **2b** cannot have structure **B**. The isotopic data can be used to discriminate between structures **C** and **D**. The band at 912.6/908.6 cm^{-1} measured for **2a** occurs in a region associated with ν(Ga–O) stretching vibrations (e.g. FGaO 943 cm^{-1} [24]). The $^{69}Ga/^{71}Ga$ isotopic splitting (4.0 cm^{-1}) is relatively large. At the same time, the wavenumber shift between the $^{16}O_2$ and $^{18}O_2$ isotopomers is also substantial [$\nu(^{16}O)/\nu(^{18}O) = 1.040$]. The corresponding band of **2b** is located at 754.6 cm^{-1}. These absorptions can be assigned to the antisymmetric ν(M–O) stretching fundamentals of **2a** and **2b**. The O–Ga–O angle, which we denote α, can be estimated on the basis of the wavenumbers measured for this mode in the case of the ^{69}Ga and ^{71}Ga isotopomers. It can be seen from Equation (1) that large isotopic shifts imply large values of α.[25]

$$\left(\frac{\nu\prime_3}{\nu_3}\right)^2 = \frac{m_M}{m_{M\prime}}\left[\frac{m_{M\prime} + m_o(1-\cos\alpha)}{m_M + m_o(1-\cos\alpha)}\right] \quad (1)$$

Upon applying this equation, it turns out that the experimental data are consistent with an O-Ga-O angle of approximately 180°. On this basis, **2a** and **2b** are most probably the linear OInO and OGaO molecules (structure **D**). This assignment is in agreement with that made in reference [4] using similar arguments. In addition, the intensity pattern observed for **2a** and **2b** is not consistent with **C**, but only with **D**. Finally, support for our assignments comes from the calculations: not only does **C** have a much higher energy than **D**, but the calculations also suggest that **C** is highly unstable toward internal conversion into **A** (see above).

The bands in the FIR region at 204.9/204.0 and 159.7 cm^{-1} can be assigned to the bending modes δ(O-Ga-O) and δ(O-In-O), respectively. These modes were detected for the first time in our work. For linear molecules and an electronic state of $^2\prod_g$, these modes are candidates for the detection of the Renner–Teller effect.[26] In the course of the deformation, the two π orbitals that host the single electron become no longer degenerate, which leads to a mode splitting. The Renner–Teller effect has been analyzed in detail, for example, in the case of OBO[27] and OCO^+[28] in the gas phase. However, it has already been shown that in the case of OBO,[29] and also of the valence isoelectronic NCO,[30] a splitting due to the Renner–Teller effect can be easily observed in the gas phase but not in an Ar matrix. We were also unable to identify any other band belonging to the linear matrix-isolated molecules in the FIR region.

It proved to be very difficult to calculate reliable wavenumbers for the vibrational modes. Due to near-instabilities of the Kohn–Sham wavefunction and the ROHF wavefunction, both B3LYP and CCSD(T) failed to reproduce the ordering of the symmetric and antisymmetric stretching modes in OGaO. Only CASSCF gives a presumably qualitatively correct result, although the deviations from the experimental numbers are distinctively larger than observed for the cyclic superoxo complex. In particular, the predicted symmetric stretching mode lies 100 cm^{-1} below the experimental value.[5] Further theoretical work will therefore be needed to obtain a better agreement. Nevertheless, the quantum-chemical calculations lend additional support to our assignment. The center of the Renner–Teller band system and the Renner–Teller parameter ε may be estimated from the two nondegenerate bending modes arising from the calculation.

Most stable isomer: Higher level calculations on GaO_2 and OGaO (isomers A and D)

Although only the cyclic isomer is formed spontaneously, we have evidence from our calculations that the linear isomer is actually energetically slightly more favorable. While DFT calculations with the B3LYP functional result in a slightly more stable cyclic isomer (by 7 $kJ\,mol^{-1}$), CCSD(T) finds the linear isomer to be more stable by 10 $kJ\,mol^{-1}$. The zero-point energy contributions calculated from the CCSD(T) frequencies favor the linear isomer by an additional 1.7 $kJ\,mol^{-1}$, such that the linear isomer is a total of 12 $kJ\,mol^{-1}$ more stable than the cyclic isomer. As the CCSD(T) frequency calculations are seemingly hampered by singlet instabilities of the underlying ROHF wavefunction (see above), one might prefer to calculate the ZPE contributions from the CASSCF frequencies. In this case the linear isomer is destabilized by around 1.6 $kJ\,mol^{-1}$, but is still a total of 8 $kJ\,mol^{-1}$ more stable than the cyclic superoxo complex.

The accuracy of the CCSD(T) calculations requires some additional investigations. From Table 5 it is evident that the

Table 5. Energy difference [kJ mol^{-1}] between the cyclic superoxo complex GaO_2 ($^2A_2$), **A**, and the linear OGaO ($^2\prod_g$), **D**, for the geometry optimized by the CCSD(T) method.

Method	ΔE_R: $GaO_2 \rightarrow$ OGaO
ROHF	+104.2
without correlation of the d orbitals	
CASSCF	+47.1
MRCI	−11.3
MRCI+Q	−17.2
ACPF	−15.3
ACPF (thr = 0.01)[a]	−15.4
with correlation of the d orbitals	
CCSD	+14.5
CCSD(T)	−9.9
CCSD[T]	−17.6
MRCI (thr = 0.01)[a]	−10.2
MRCI (thr = 0.01)[a]+Q	−22.6
ACPF (thr = 0.01)[a]	−18.2
AQCC (thr = 0.01)[a]	−18.0

[a] Selection threshold, see computational details.

linear isomer has a much higher energy than the cyclic one at the uncorrelated level (ROHF), and even at the CCSD level the calculations predict the linear isomer to be 15 kJ mol^{-1} less stable. Only at the CCSD(T) level do we arrive at the result that the linear isomer is more stable. The alternative triples correction [T][31] may be used to estimate the reliability of the CCSD(T) numbers. The result differs by almost 8 kJ mol^{-1} (see Table 5). This indicates that some near-degeneracy effects are present—in particular for the linear isomer—and it appeared therefore interesting to pursue this case further with the aid of multireference methods. CASSCF only includes static correlation and the parts of dynamic correlation covered by excitations within the selected active space. As pointed out above, the active spaces for the linear and the cyclic isomer are not completely compatible, which results in a too strong stabilization of the cyclic compound (see Table 5). However, we still have a better starting point for the subsequent correlation treatment than was the case with ROHF.

Excluding the d electrons from the MR-CI correlation treatment we find that the linear isomer is again more stable by 11 kJ mol^{-1}, which increases to around 15 kJ mol^{-1} when using methods that correct for the size-extensivity error of MR-CI by approximating the effect of disconnected quadruple excitations. If we want to include the correlation of the d-electrons, we have to select the dominant reference configurations in the CASSCF wavefunction to keep the problem tractable. The effect of this selection was tested for ACPF without d-electron correlation and found to be 0.1 kJ mol^{-1}, which is sufficiently small. The dispersion interaction of the Ga 3d shell with the oxygen atoms stabilizes the linear isomer further, as both AQCC and ACPF give a value of 18 kJ mol^{-1}, which is close to the CCSD[T] result. The size-extensivity corrections, however, are larger at this level (around 8 kJ mol^{-1}).

In summary, the calculations indicate that the linear isomer defines the global energy minimum of all possible GaO_2 isomers, closely followed by the cyclic superoxide. For a more precise answer we would need to go to the CCSDT level (or beyond), to use quadruple-zeta, or better, basis sets, and possibly to include a further core-correlation, which currently is beyond realization for a system of this size.

Normal coordinate analysis for linear OGaO

The observed wavenumbers can be used to determine the force constants *f*(MO), the interaction force constants *f*-(MO,MO), which show the amount of coupling between the two M−O bonds, and the force constant for bending *f*-(OMO). The details of the normal coordinate analysis are included in the Supporting Information. The force constants *f*(MO) and *f*(MO,MO) are included in Table 6, which also contains the force constants determined for other OMO molecules (M being B,[27,29,32] Al,[33] Tl,[5] C,[34] Si,[35] Ge,[36] Sn,[37] and Pb[38]) and for CO_2^+.[34] Once *f*(MO) and *f*-(MO,MO) have beene determined, the wavenumber of the symmetric stretching mode, ν_1, can be calculated; we obtained estimates of 821 and 720 cm^{-1} for ν_1(GaO) and ν_1-(InO), respectively.[5] We want to point out here that anharmonicity effects were neglected and therefore this is an estimate, with an uncertainty of a few wavenumbers. Nevertheless, our analysis achieves a more or less complete vibrational characterization of the molecules. The wavenumbers of the symmetric ν(Ga−O) and ν(In−O) stretches are lower than those of the antisymmetric stretches. We have already mentioned that the bands observed for the antisymmetric ν-(M−O) stretches of $^{16}OM^{18}O$ are blue-shifted with respect to the center of the wavenumbers of the corresponding modes in the $^{16}OM^{16}O$ and $^{18}OM^{18}O$ isotopomers. This blue-shift can be explained by the coupling with the symmetric stretch in $^{16}M^{18}O$, which has a lower wavenumber.

It does not come as a surprise that *f*(MO) is smaller in OInO than in OGaO (454 N m^{-1} in OInO versus 586 N m^{-1} in OGaO). The higher ionic bond character in OInO might also be the main reason for the reduced interaction force constant *f*(MO,MO) (34 N m^{-1} in OInO and 50 N m^{-1} in OGaO). Finally, useful information is contained in the force constant for angle deformation, *f*(OMO). Again, this force constant is significantly smaller in OInO than in OGaO (9 versus 14×10^{-20} J).[39] Since bending leads especially to a weakening of any possible π-interaction, this trend might again imply that the π-interaction in OGaO is larger than in OInO.

CO_2^+, which is formally valence isoelectronic with GaO_2 and InO_2, has been studied intensively.[28] This species is linear, like GaO_2 and InO_2, and exhibits a $^2\prod_g$ electronic ground state. The force constant in CO_2^+ is smaller than that of CO_2 by a factor of about 1.5 (1049 versus 1617 N m^{-1}), but nevertheless somewhat larger than *f*(BO) in BO_2 (1049 versus 750 N m^{-1}).[29] The force constants are higher for OMO compounds of Group 14 than for the corresponding compounds of Group 13 and the same period in the periodic table. To better visualize these trends, they are plotted in Figure 6. The force constant decreases dramatically from CO_2 to SiO_2 (from 1617 to 920 N m^{-1}).[35] From

Table 6. Experimental and calculated wavenumbers [cm^{-1}] and force constants [all in $N\,m^{-1}$ except for F_{22} (in $10^{-20}J$)[39]] for OMO molecules.

		OBO		OAlO	OGaO	OInO	OTlO	OCO^+	OCO
reference	[27a][a]	[27b][a]	[29][b]	[33][b]	this work[b]	this work[b]	[5][b]	[34][a]	[34][a]
ν_1	1070	1068.9	–	862[c]	821[c]	720[c]	696[c]	1280	1345.0
ν_2	464	449.9	398.2	–	204.9	159.7	–	510	667
ν_3	1322	1336.6	1299.3	1129.5	912.6	754.6	698.0	1469	2349
F_{11}	1079	1077	–	701[c]	635[c]	488[c]	457[c]	1544	1705
F_{22} [δ(OMO)]	26	24	19	–	14	9	–	33	57
F_{33}	421	431	407	550	536	420	397	555	1561
f(MO)	750	754	–	626[c]	586[c]	454[c]	427[c]	1049	1617
f(MO,MO)	329	323	–	75[c]	50[c]	34[c]	30	495	143

	OSiO	OGeO	OSnO	OPbO
reference	[35,36][b]	[36][d]	[37][e]	[38][b]
ν_1	–	888.3	827[c]	763[c]
ν_2	272.5	197.6	–	–
ν_3	1416.5	1074.1	863.1	764.8
F_{11}	–	744	644[c]	549[c]
F_{22}[δ(OMO)]	16	13	–	–
F_{33}	882	759	554	478[c]
f(MO)	920[f]	751	599[c]	514[c]
f(MO,MO)	40[f]	–8	45[c]	36[c]

[a] Gas phase. [b] Ar matrix. [c] Estimated from ν_3 of $^{16}OM^{16}O$ and $^{16}OM^{18}O$. [d] Ar matrix ($\nu_{2,3}$), CH_4 matrix (ν_1). [e] Kr matrix. [f] Estimated from known values for siloxanes and FAlO.

OBO to OAlO the force constant also decreases, although less dramatically (from 750 to 626 $N\,m^{-1}$). For both the third and the fourth main group the decrease is much smaller between the third and the fourth period in the periodic table (from OAlO to OGaO and from OSiO to OGeO).[40]

The trends of the interaction force constants are also visualized in Figure 6. As expected, *f*(MO,MO) generally decreases down the group. From OBO to OAlO, *f*(MO,MO) decreases by a factor of about 4.3 (323 versus 75 $N\,m^{-1}$). In OGaO, *f*(GaO,GaO) amounts to around 50 $N\,m^{-1}$. Thus, the decrease is again much smaller from OAlO to OGaO. It has already been mentioned that the interaction force constant is very sensitive to the covalent bond contributions. Finally, Figure 6 shows the trends for the force constant for angle deformation, *f*(OMO). Again, in general *f*(OMO) decreases down the group. Unfortunately, there are no experimental values available for OAlO, and the accuracy of the calculations carried out to date is questionable.

Description of the bond properties in the linear OMO molecules

The bond order, *N*, of the M–O bond in linear OMO can be estimated on the basis of the formula introduced by Siebert (see Equation (2)).[41] In this formula, f_1 is the *f*(MO) force constant of a reference molecule that is known to contain a single bond and f_N is the *f*(MO) force constant in our linear OMO molecules, as determined above by normal coordinate analysis. As reference molecules, we chose the bent HMOH radical species, for which vibrational data (measured in Ar matrices) are well known.[42] Possible π-contributions of the M–O bond in these M^{II} radicals should be very small.

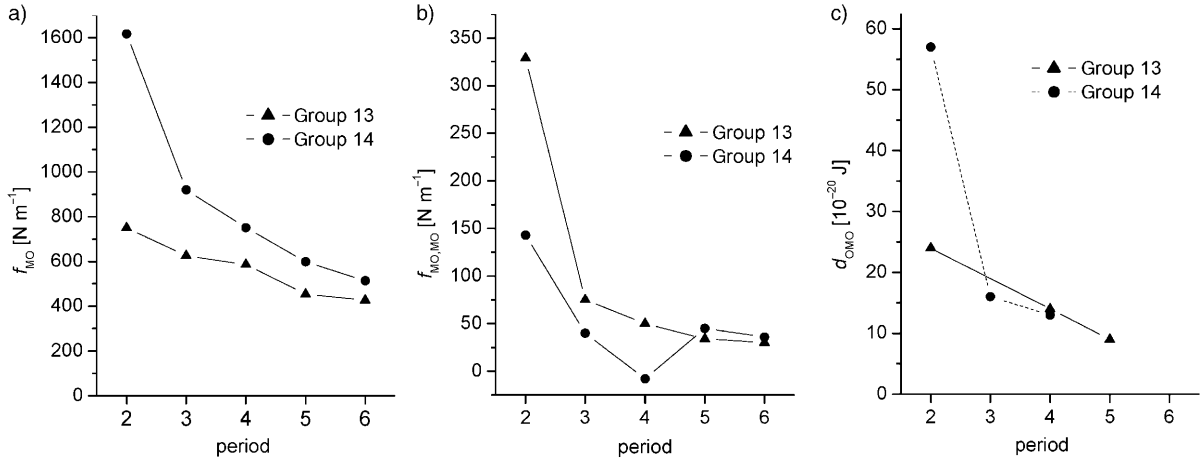

Figure 6. Force constants a) *f*(MO), b) *f*(MO,MO), and c) *f*(OMO) as derived for linear OEO molecules, where E is a Group 13 or 14 element.

$$N = 0.57 \cdot \frac{f_N}{f_1} + 0.43 \cdot \sqrt{\frac{f_N}{f_1}} \quad (2)$$

Table 7 contains the bond order calculated for OAlO, OGaO, and OInO from Equation (2). For all three molecules the bond order turns out to be between 1 and 2, in good agreement with the predictions on the basis of the MO diagram (see below). The bond order increases slightly from 1.4 in OAlO to 1.6 in OGaO. This increase does not come as a surprise since the bonds in OAlO should be more polar than those in OGaO. However, the results suggest that the bond order in OInO is similar to that in OGaO. This is not in line with the expectations and shows the limitations of this simple equation. Nevertheless, the estimated bond order is in line with what we can deduce from simple molecular orbital and valence bond theory.

Table 7. Estimated bond orders in the linear OMO molecules (M = Al, Ga or In) according to the formula introduced by Siebert (see text for further explanation).

	HAlOH[a]	HGaOH[a]	HInOH[a]	OAlO[b]	OGaO[c]	OInO[c]
ν_{MO}	817.9	646.4	548	1129.5/862	912.6/821	754.6/720
f_{MO}	417	337	262	626	586	454
Bond order	1.00	1.00	1.00	1.4	1.6	1.6

[a] Reference [43]. [b] Reference [33]. [c] This work

An inspection of the frontier orbitals of GaO_2 and InO_2 shows similarities with CO_2^+, which is formally valence isoelectronic with these species and also exhibits a linear structure. The unpaired electron resides in a nonbonding orbital. Formally, two bonding σ orbitals and a degenerate pair of bonding π orbitals are occupied. This would suggest a bond order of two per bond, but in contrast to $[OCO]^+$ the π-orbitals have larger amplitudes on the oxygen atoms, that is, partial oxygen lone-pair character.

The bond properties may also be rationalized with the help of Lewis structures. One may consider the following six structure formulae (a), (a′), (b), (b′), (c), and (c′). The unpaired electron is always assumed to reside in a lone pair, as suggested by MO theory. Formulae (a) and (a′) are the most important structures in the case of $[OCO]^+$—they give an electron octet at the central atom—but for Ga a negative partial charge would result. The above-mentioned partial lone-pair character of the p frontier orbitals and the positive partial charge on Ga/In arising in the calculations suggest that mainly structures (b)/(b′) and partially also (c)/(c′) describe the bonding in linear OMO.

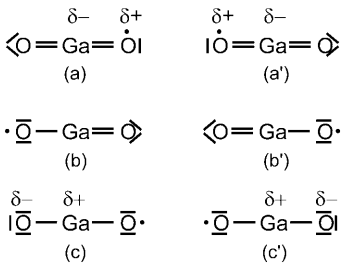

Information about the reaction mechanism

The experiments show that the formation of cyclic GaO_2 proceeds spontaneously even at very low temperatures, which means that the activation barrier for this process should be close to zero. The results of the experiments using mixtures of $^{16}O_2$ and $^{18}O_2$ indicate that cyclic GaO_2 is formed from Ga and O_2 in a concerted reaction (not in a radical mechanism via GaO and O) However, isomerization to linear OGaO is subject to a substantial barrier. Additional quantum-chemical calculations were therefore performed to obtain more information about the mechanism.

The reaction can be divided into two steps: formation of the cyclic GaO_2 species from Ga atoms and O_2 and the photoisomerization of cyclic GaO_2 into linear OGaO. This pathway has already been discussed in previous work.[4,5] However, we report in the following on quantum-chemical calculations that lead to a more detailed understanding of the reaction mechanism.

Reaction to cyclic GaO_2: Figure 7 shows the dependence of the O–O distance, the dipole moment, and the potential energy for the system $Ga + O_2$ on the reaction coordinate, which is defined as the distance (d(Ga–O_2)) between the Ga atom and the O_2 centroid. It can be seen that, as O_2 and Ga approach each other, the energy and the O–O distance do not change significantly for d(Ga–O_2) values greater than 300 pm. For values of the reaction coordinate smaller than 270 pm, the O–O distance is significantly elongated. At the same time, the energy decreases. This means that there is an abrupt change in the structure during the approach. This change in structure is, however, not accompanied by a significant energy barrier. Figure 7 also shows the behavior of the dipole moment during the approach. Again, there is an abrupt change of the dipole moment, which shows that the electronic properties change. This behavior resembles that expected for the "harpooning" mechanism, for which an electron jumps from one group of atoms to another at a well-defined distance. This distance, d, can be estimated from Equation (3), in which the ionization energy of Ga, I(Ga), is 5.999 eV and the electron affinity of O_2, $E_A(O_2)$, is 0.45 eV. This equation leads to $d = 260$ pm, a value that is only about 7% smaller than that calculated in our quantum-chemical calculations.

$$I(\mathrm{Ga}) - E_A(O_2) = \frac{e^2}{4\pi\varepsilon_0 d} \quad (3)$$

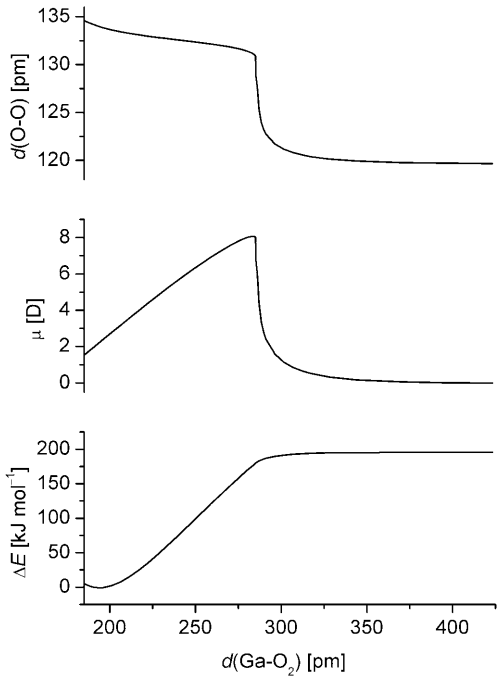

Figure 7. Dependence of the calculated (RASSCF, see text) d(O–O), dipole moment, and relative energy on the reaction coordinate d(Ga–O_2) for the reaction between Ga and O_2 leading to the cyclic superoxo complex GaO_2.

In the course of the approach of the Ga atom toward the O_2 molecule an attractive interaction is established between the p orbital at the Ga atom, which contains one electron, and the π^* orbitals at the O_2 unit, which are both half-filled in the $^3\Sigma_u^-$ electronic ground state of O_2. If the approach takes place in the xz plane and z is the reaction coordinate, the bond is formed between the Ga p_x orbital and the O_2 π^*_z orbital, while the π^*_y orbital remains inactive. This attractive interaction, which is active prior to the abrupt electron transfer, is responsible for the absence of a reaction barrier. The $(p_x+\pi^*_z)$ bonding orbital already has an occupation number of 1.8 prior to the electron transfer [that is, at $d(\mathrm{Ga{-}O_2}) > 270$ pm], but the character of the bond is still covalent as both contributing orbitals still have nearly equal weight. As the fragments further approach each other, the bonding molecular orbital assumes nearly exclusive O_2 π^*_z character. This corresponds to the transfer of one electron from Ga to the O_2 moiety, resulting in dominant ionic bonding in cyclic GaO_2.

Isomerization to linear OGaO: The main aim of this section is to explain the reasons for the large barrier for isomerization from cyclic GaO_2 to linear OGaO. The presence of a barrier is responsible for the failure to observe the linear OGaO molecule immediately upon deposition, since the isomerization of cyclic GaO_2 into the linear isomer is exothermic according to our best calculations.

Figure 8 shows a correlation diagram for the isomerization reaction. Bending the linear molecule reduces its symmetry to C_{2v}, and the two degenerate $\prod_g$ orbitals of the linear

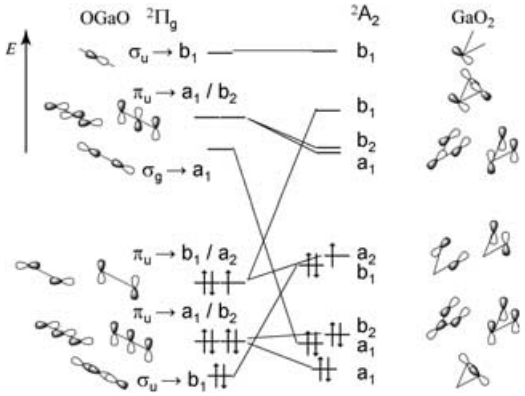

Figure 8. Correlation diagram for the isomerization of cyclic into linear GaO_2. The Ga 4s orbital has been omitted for clarity.

OGaO molecule split into two orbitals of a_2 and b_1 symmetry, respectively. Thus, the degenerate ground state of OGaO splits into two hypersurfaces of either $^2A_2$ or $^2B_1$ symmetry, with the latter being lower in energy. The σ_u orbital and the two degenerate π_u orbitals transform into b_1 and a_1, and b_2 respectively. As can be seen from the correlation diagram, a bonding a_1 orbital of cyclic GaO_2 correlates with an unoccupied orbital of linear OGaO; instead, a b_1 orbital becomes occupied. Basically, as Ga inserts into the O–O bond the bonding σ orbital of O_2 is emptied and the antibonding σ* orbital is filled instead. The configuration of cyclic GaO_2 thus corresponds to an excited state of linear OGaO; that is, the reaction is symmetry-forbidden in the sense of Woodward and Hoffman[43] and normally associated with a significant barrier.

To get more quantitative information about the barrier, potential energy hypersurfaces were calculated at the CASSCF level. Figure 9a shows a potential energy map for GaO_2 with the assumption that the system remains in the $^2A_2$ electronic state. We note two features: First, the transition state (indicated by the circle in Figure 9a) lies at considerably higher energy than the cyclic superoxo compound (more than 300 kJ mol^{-1} above). Even though CASSCF fails to reproduce the energy separation between OGaO and cyclic GaO_2 by about 50 kJ mol^{-1}, the calculated data allow us to estimate a barrier height that cannot be overcome under matrix conditions. Second, the reaction path towards the transition state includes a significant stretch of the O_2 bond, which suggests that vibrationally hot O_2 is required for a reactive collision, whereas a collision with nonexcited O_2 is purely repulsive.

The picture does not significantly change if we consider an alternative mechanism which includes internal conversion from the $^2A_2$ energy hypersurface to the $^2B_1$ surface. The latter is, as mentioned above, the lower sheet of the pair of energy surfaces leading to the degenerate $^2\prod_g$ state of linear OGaO. The energy hypersurface for the $^2B_1$ state of linear OGaO and for the $^2A_2$ state of cyclic GaO_2 are shown together in Figure 9b. These two surfaces intersect and only the parts of the surfaces with the lowest energy are visual-

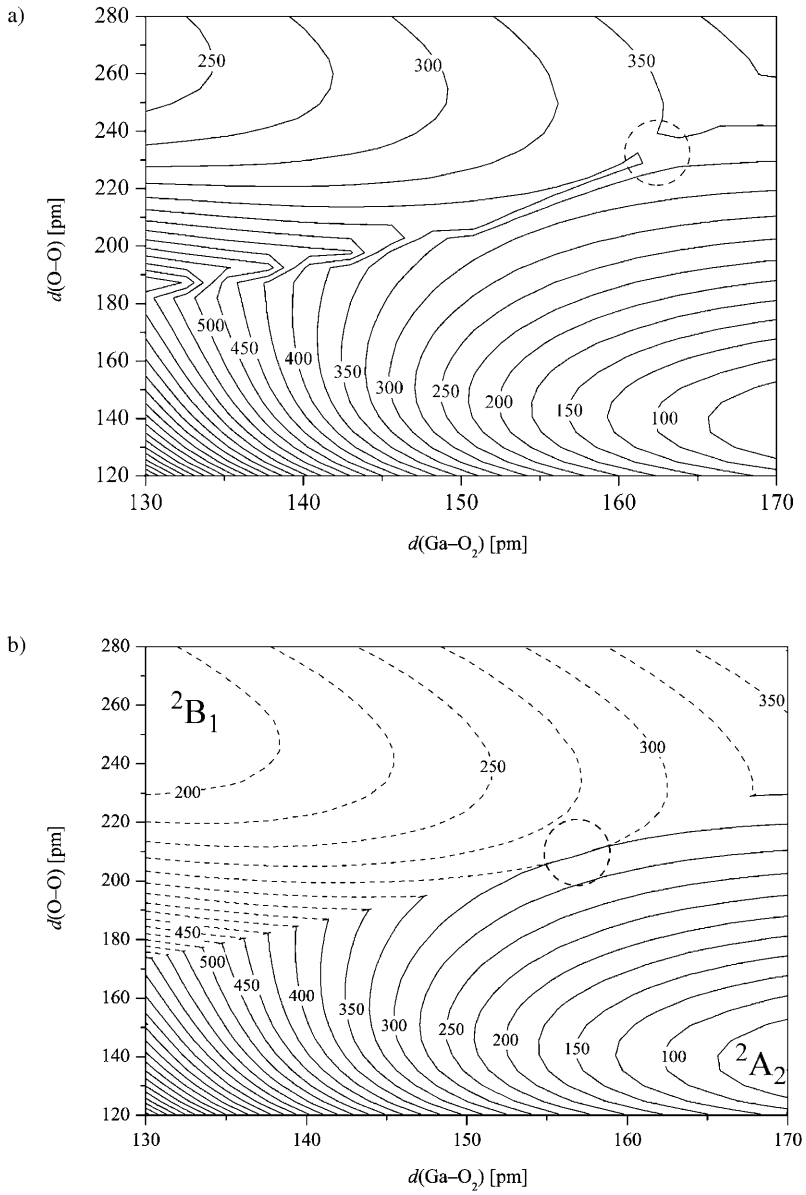

Figure 9. a) Plot of the calculated (CASSCF, see text) $^2A_2$ energy hypersurface near the transition point for the isomerization of cyclic to linear GaO_2. b) Plot of the calculated $^2A_2$ and $^2B_1$ energy hypersurfaces near the transition point for the isomerization of cyclic to linear GaO_2.

ized. A circle marks the area where the system might convert from the $^2A_2$ to the $^2B_1$ potential energy hypersurface with minimal energy. Again, the barrier comes out to be around 300 kJ mol^{-1}. Thus, the possible conversion to another electronic state does not lead to a significant decrease of the activation barrier.

In summary, the calculations show that isomerization of cyclic GaO_2 to linear OGaO, although presumably an exothermic process, cannot proceed thermally, especially not under matrix conditions, because of an energy barrier that is apparently higher than the $Ga + O_2 \rightarrow GaO_2$ reaction energy. It is worth mentioning that this energy is close to the energy required for a radical mechanism leading first to GaO and O atoms (ca. 300 kJ mol^{-1} both at the CASSCF and the CCSD(T) level).

Conclusion

The cyclic superoxo complex MO_2 and the linear OMO (M = Ga or In) molecules are the products of the spontaneous and photolytically activated matrix reactions between the metal atoms and O_2. IR and Raman data have been used to characterize these species, which were already observed in previous work.[2–4] The force constants of the linear OMO species were calculated by normal coordinate analysis and compared to those of other linear triatomic species. Quantum-chemical calculations using coupled-cluster and multireference methods indicate that the linear OMO is energetically slightly favored over its cyclic isomer. The bond properties of these species have been discussed. The Ga–O bond order is in between one and two. Quantum-chemical calculations were carried out which provide detailed information about the reaction mechanisms. The calculations agree with the experiments that formation of the cyclic superoxo complex GaO_2 from Ga atoms and O_2 occurs without a significant reaction barrier. In the course of the approach of the two reactants, an abrupt charge-transfer is observed. This marks the point at which one electron jumps from the Ga atom onto the O_2 unit. Accordingly, the bonding in the product is dominated by ionic contributions. Although linear OGaO exhibits a lower energy, photolysis is needed to isomerize the superoxo complex into the linear form. The calculations indeed show that isomerization of the molecule in its electronic ground state is subjected to a substantial barrier of around 300 kJ mol^{-1}.

The results of this work are of relevance to metal-based oxidation processes as they show the ability of metal atoms to insert into the strong O–O bond. The evaluation of the mechanisms for these processes is important to understand the oxidation of metals.

Acknowledgments

The authors thank the Deutsche Forschungsgemeinschaft and the Fonds der Chemischen Industrie for financial support.

[1] A. Al-Muhanna, L. J. Mawst, D. Botez, D. Z. Garbuzov, R. U. Martinelli, J. C. Connolly, *Appl. Phys. Lett.* **1998**, *73*, 1182.
[2] M. J. Zehe, D. A. Lynch, Jr., B. J. Kelsall, K. D. Carlson, *J. Phys. Chem.* **1979**, *83*, 656.
[3] L. V. Serebrennikov, S. B. Ozin, A. A. Maltsev, *J. Mol. Struct.* **1982**, *81*, 25.
[4] a) T. R. Burkholder, J. T. Yustein, L. Andrews, *J. Phys. Chem.* **1992**, *96*, 10189; b) L. Andrews, G. P. Kushto, J. T. Yustein, E. Archibong, R. Sullivan, J. Leszczynski, *J. Phys. Chem. A* **1997**, *101*, 9077.
[5] After the final version of this manuscript was accepted, anion photoelectron spectra of linear OGaO were published, which estimated the Σ_g mode to occur at $760 \pm 30\ cm^{-1}$: G. Meloni, S. M. Sheeham, D. M. Neumark, *J. Chem. Phys.* **2005**, *122*, 074317
[6] Y. Bu, D. Chan, X. Song, *Int. J. Quantum Chem.* **2001**, *81*, 222.
[7] E. F. Archibong, A. St-Amant, *Chem. Phys. Lett.* **1998**, *284*, 331.
[8] See, for example: H.-J. Himmel, A. J. Downs, T. M. Greene, *Chem. Rev.* **2002**, *102*, 4191.
[9] a) R. Ahlrichs, M. Bär, M. Häser, H. Horn, C. Kölmel, *Chem. Phys. Lett.* **1989**, *162*, 165; b) K. Eichkorn, O. Treutler, H. Öhm, M. Häser, R. Ahlrichs, *Chem. Phys. Lett.* **1995**, *240*, 283; c) K. Eichkorn, O. Treutler, H. Öhm, M. Häser, R. Ahlrichs, *Chem. Phys. Lett.* **1995**, *242*, 652; d) K. Eichkorn, F. Weigend, O. Treutler, R. Ahlrichs, *Theor. Chem. Acc.* **1997**, *97*, 119; e) F. Weigend, M. Häser, *Theor. Chem. Acc.* **1997**, *97*, 331; f) F. Weigend, M. Häser, H. Patzelt, R. Ahlrichs, *Chem. Phys. Lett.* **1998**, *294*, 143.
[10] T. Helgaker, H. J. A. Jensen, P. Jørgensen, J. Olsen, K. Ruud, H. Ågren, A. A. Auer, K. L. Bak, V. Bakken, O. Christiansen, S. Coriani, P. Dahle, E. K. Dalskov, T. Enevoldsen, B. Fernandez, C. Hättig, K. Hald, A. Halkier, H. Heiberg, H. Hettema, D. Jonsson, S. Kirpekar, R. Kobayashi, H. Koch, K. V. Mikkelsen, P. Norman, M. J. Packer, T. B. Pedersen, T. A. Ruden, A. Sanchez, T. Saue, S. P. A. Sauer, B. Schimmelpfennig, K. O. Sylvester-Hvid, P. R. Taylor, and O. Vahtras; DALTON—an electronic structure program, release 1.2, **2001**.
[11] a) C. Hampel, K. Peterson, H. J. Werner, *Chem. Phys. Lett.* **1992**, *190*, 1; b) P. J. Knowles, H. J. Werner, *Chem. Phys. Lett.* **1985**, *115*, 259; c) P. J. Knowles, H. J. Werner, *Chem. Phys. Lett.* **1988**, *145*, 514; d) H. J. Werner, P. J. Knowles, *J. Chem. Phys.* **1985**, *82*, 5053; e) H. J. Werner, P. J. Knowles, *J. Chem. Phys.* **1988**, *89*, 5803.
[12] a) A. D. P. Becke, *Phys. Rev. A* **1988**, *38*, 3098; b) C. Lee, W. Yang, R. G. Parr, *Phys. Rev. B* **1988**, *37*, 785; c) A. D. Becke, *J. Chem. Phys.* **1993**, *98*, 5648.
[13] a) A. Schäfer, C. Huber, R. Ahlrichs, *J. Chem. Phys.* **1994**, *100*, 5829; b) A. Bergner, M. Dolg, W. Kuechle, H. Preuss, *Mol. Phys.* **1993**, *80*, 1431; c) T. Leininger, A. Berning, A. Nicklass, H. Stoll, H.-J. Werner, H.-J. Flad, *Chem. Phys.* **1997**, *217*, 19.
[14] See: A. Köhn, H.-J. Himmel, B. Gaertner, *Chem. Eur. J.* **2003**, *9*, 3909.
[15] K. Raghavachari, G. W. Trucks, J. A. Pople, M. Head-Gordon, *Chem. Phys. Lett.* **1989**, *157*, 479.
[16] a) J. Olsen, B. O. Roos, P. Jørgensen, H. J. Aa. Jensen, *J. Chem. Phys.* **1988**, *89*, 2185; b) H. J. Aa. Jensen, P. Jørgensen, T. Helgaker, J. Olsen, *Chem. Phys. Lett.* **1989**, *162*, 355; c) P.-Å. Malmqvist, A. Rendell, B. O. Roos, *J. Phys. Chem.* **1990**, *94*, 5477.
[17] a) S. R. Langhoff, E. R. Davidson, *Int. J. Quantum Chem.* **1974**, *8*, 61; b) P. Bruna, S. D. Peyerimhoff, R. J. Buenker, *Chem. Phys. Lett.* **1980**, *72*, 278.
[18] R. J. Gdanitz, R. Ahlrichs, *Chem. Phys. Lett.* **1988**, *143*, 413.
[19] a) P. G. Szalay, R. J. Bartlett, *Chem. Phys. Lett.* **1993**, *214*, 481; b) P. G. Szalay, R. J. Bartlett, *J. Chem. Phys.* **1995**, *103*, 3600.
[20] B. Gaertner, A. Köhn, H.-J. Himmel, unpublished results.
[21] R. D. Lafleur, J. M. Parnis, *J. Phys. Chem.* **1992**, *96*, 2429.
[22] H.-J. Himmel, B. Gaertner, *Chem. Eur. J.* **2004**, *10*, 5936.
[23] J. A. Creighton, E. R. Lippincott, *J. Chem. Phys.* **1964**, *40*, 1779.
[24] H. Schnöckel, H. J. Göcke, *J. Mol. Struct.* **1978**, *50*, 281.
[25] O. Redlich, *Z. Phys. Chem. Abt. B* **1935**, *28*, 371.
[26] See, for example: R. Renner, *Z. Phys.* **1934**, *92*, 172.
[27] a) J. W. C. Johns, *Can. J. Phys.* **1961**, *39*, 1738; b) K. G. Weyer, R. A. Beaudet, R. Straubinger, H. Walther, *Chem. Phys.* **1980**, *47*, 171; c) K. Kawaguchi, E. Hirota, *J. Mol. Spectrosc.* **1986**, *116*, 450; d) K. Kawaguchi, E. Hirota, C. Yamada, *Mol. Phys.* **1981**, *44*, 509.
[28] a) M. Brommer, G. Chambaud, E. A. Reinsch, P. Rosmus, A. Spielfiedel, N. Feautrier, H. J. Werner, *J. Chem. Phys.* **1991**, *94*, 8070; b) J. Liu, W. Chen, C. W. Hsu, M. Hochlaf, M. Evans, S. Stimson, C. Y. Ng, *J. Chem. Phys.* **2000**, *112*, 10767; c) J. Liu, W. Chen, M. Hochlaf, X. Qian, C. Chang, C. Y. Ng, *J. Chem. Phys.* **2003**, *118*, 149.
[29] T. R. Burkholder, L. Andrews, *J. Chem. Phys.* **1991**, *95*, 8697.
[30] D. E. Milligan, M. E. Jacox, *J. Chem. Phys.* **1967**, *47*, 5157.
[31] M. Urban, J. Noga, S. J. Cole, R. J. Bartlett, *J. Chem. Phys.* **1985**, *83*, 4041.
[32] K. G. Weyer, R. A. Beaudet, R. Straubinger, H. Walther, *Chem. Phys.* **1980**, *47*, 171.
[33] L. Andrews, T. R. Burkholder, J. T. Yustein, *J. Phys. Chem.* **1992**, *96*, 10182.
[34] G. Herzberg, *Molecular Spectra and Molecular Structure, III, in Electronic Spectra and Electronic Structure of Polyatomic Molecules*, van Nostrand, Princeton, **1950**.
[35] a) H. Schnöckel, *Angew. Chem.* **1978**, *90*, 638; *Angew. Chem. Int. Ed. Engl.* **1978**, *17*, 616; b) H. Schnöckel, *Z. Anorg. Allg. Chem.* **1980**, *460*, 37.
[36] M. Friesen, M. Junker, H. Schnöckel, *J. Chem. Phys.* **2000**, *112*, 1782.
[37] A. Bos, J. S. Ogden, *J. Phys. Chem.* **1973**, *77*, 1513.
[38] G. V. Chertihin, L. Andrews, *J. Chem. Phys.* **1996**, *105*, 2561.
[39] After division by 10^{-20} m for normalization, force constants of 4 and $9\ N\,m^{-1}$ result for the bending force constants.
[40] M. Friesen, M. Junker, H. Schnöckel, *J. Chem. Phys.* **2000**, *112*, 1782.
[41] H. Siebert, *Anwendungen der Schwingungsspektroskopie in der anorganischen Chemie*, Springer Verlag, Berlin, **1966**.
[42] R. H. Hauge, J. W. Kauffman, J. L. Margrave, *J. Am. Chem. Soc.* **1980**, *102*, 6005.
[43] R. B. Woodward, R. Hoffmann, *Angew. Chem.* **1969**, *81*, 797; *Angew. Chem. Int. Ed. Engl.* **1969**, *8*, 781.

Received: February 8, 2005
Published online: July 12, 2005

